Mirror-symmetry-protected topological superfluid and second-order topological superfluid in bilayer fermionic gases with spin-orbit coupling

Beibing Huang,* Gaixia Luo,† and Ning Xu‡
Department of Physics, Yancheng Institute of Technology, Yancheng 224051, China

(Received 6 March 2019; published 2 August 2019)

The experimental realizations of spin-orbit coupling (SOC) in cold atom gases put topological superfluids (TSs) under the spotlight. The topological protection of suggested superfluid models comes from the local antiunitary symmetries of ten Altland-Zirnbauer symmetry classes. In this paper we theoretically study a two-dimensional BDI model describing spin-orbit-coupled bilayer fermionic gases with *s*-wave interaction to realize mirror-symmetry- (nonlocal and unitary) protected gapped TS, beyond the paradigms suggested before. This gapped phase not only shows linearly dispersive Majorana zero modes on mirror invariant one-dimensional boundaries, but also shows Majorana corner states to realize the second-order TS (TS2) with *s*-wave pairing, which is explicitly different from the nonconventional pairings in the suggested systems to realize TS2. Generally, engineering the single-particle band structures should be easier than directly engineering the complicated pairings. Considering the tremendous progress in manipulating cold atom systems, our work provides a possible route (by engineering the single-particle physics, such as SOC) to realize mirror-symmetry-protected gapped TS and TS2 in cold fermionic systems in the future.

DOI: 10.1103/PhysRevA.100.023602

I. INTRODUCTION

Majorana fermions [1], which can be regarded as zero-energy Bogoliubov quasiparticles on the boundaries of topological superfluids (TSs), are self-Hermitian anyons satisfying non-Abelian statistics and the basic building blocks for fault-tolerant topological quantum computation [2–4]. With the realization of spin-orbit coupling (SOC) generated by the laser-induced Raman transitions between atomic hypefine states [5–13], ultracold degenerate Fermi gases have become a brand-new experimental playground to explore the exotic quantum phases in condensed-matter physics. Combined with the attractive two-body interaction, SOC can induce effective *p*-wave pairings and drive the system into TSs protected by the local antiunitary symmetries of ten Altland-Zirnbauer symmetry classes [14,15]. Some suggested two-dimensional models include D class TS with Rashba SOC and Zeeman field [16–19], C class TS in Haldane-Hubbard model [20], and DIII class TS in Bose-Fermi mixtures [21].

Conceptually the notion of TSs has been extended to include a new class of topological phases without gapless Majorana boundary states, dubbed as higher-order TSs [22–30]. A second-order TS (TS2) is a d-dimensional system with topologically nontrivial gapped $(d-1)$-dimensional boundaries such that there are protected low-energy modes at the $(d-2)$-dimensional boundaries. In other words, a TS2 in $2d$ has Majorana corner states (MCSs), i.e., Majorana fermions bound at the intersection of two boundaries. Some experimental setups for TS2 have been suggested theoretically in proximity-induced systems, including $2d$ topological insulator grown on a cuprate superconductor or $s_{\pm}$-wave Fe-based superconductor [28,30], a cuprate superconductor or Rashba semiconductor placed on top of a time-reversal-invariant *p*-wave superconductor [29], and a cuprate superconductor sandwiched between two Fe-based superconductors $FeTe_{0.55}Se_{0.45}$ [29].

Although some possible systems for TS2 have been proposed, the pairings in the suggested models [28–30] are unconventional. Usually the interaction between ultracold atoms is in *s*-wave channel; thus a natural question emerges: is it possible to engineer TS2 in ultracold fermionic gases with *s*-wave interaction by engineering single-particle band structures? Generally, engineering the single-particle band structures should be easier than directly engineering the complicated pairings. In this paper we give a positive answer to this question by the self-consistent mean-field analyses on a theoretic model with *s*-wave pairing. Our suggested model can be mapped onto a bilayer model in the cold fermionic gases with π (0) phase difference for SOC along k_y (k_x) direction between two layers and show gapped TS protected by an emergent mirror symmetry (MS) (nonlocal and unitary). This MS-protected TS implies Majorana zero modes (MZMs) on the mirror reflection invariant boundaries, while other boundaries are gapped [31–34]. Considering one pair of gapped boundaries, which are not left invariant but mapped onto each other under mirror reflection, the topological nontriviality of the bulk guarantees that the mirror-symmetry-breaking mass terms on these boundaries are unique and exhibit gaps of opposite signs [23,25]. As a result, the intersection of such a pair of boundaries corresponds to a domain wall and naturally leads to MCSs to realize TS2. As a matter of fact, these MCSs are also robust when the system is rotated, such that there are no longer any mirror-related boundaries [23,25].

*hbb4236@ycit.edu.cn
†GaixiaLuo@163.com
‡nxu@ycit.cn

The paper is organized as follows. In Sec. II, we present our theoretic model and Bogoliubov–de Gennes (BdG) mean-field theory. In Sec. III, the mean-field ground state and the phase diagram of the model are self-consistently determined by minimizing the thermodynamic potential. We find that the model shows two kinds of topologically nontrivial bulk phases: gapped TS and gapless nodal TSs. An interesting result is that gapless nodal TSs are also topologically nontrivial in the mirror subspaces; as a result all TSs can be distinguished from the number of Dirac points and topological winding numbers in two mirror subspaces. In Sec. IV the boundary states and corner states are studied. In the topological gapped phase, there are linearly dispersive MZMs on the mirror-invariant boundaries, while in the gapless topological phases there are Majorana flat bands (MFBs). Especially we also observe the coexistence of two kinds of boundary states mentioned above. For $(d-2)$-dimensional boundaries, these phases also accommodate MZMs. For the gapped TS, these MZMs are definitely localized around the corners to realize MCSs, while, for gapless TSs, the wave functions of MZMs more or less leak into the interior of the system owing to MFBs on the $(d-1)$-dimensional boundaries. In Sec. V, we briefly discuss the stability of the ground state of our model about two more general mean-field *Ansätze* and how to detect experimentally all phases realized in our model in the ultracold atom environment. Finally, we draw the conclusions in Sec. VI. Our work provides a possible route to realize MS-protected TSs and TS2 in an ultracold fermionic system in the future.

II. MODEL

We consider a spin-orbit-coupled bilayer fermionic system, which is described by the Hamiltonian

$$\begin{aligned} H = & \sum_{\mathbf{k},i,\sigma\sigma'} c^{\dagger}_{\mathbf{k}i\sigma}[\epsilon_{\mathbf{k}} + \Gamma\sigma_z + \rho_{\mathbf{k}i}]_{\sigma\sigma'} c_{\mathbf{k}i\sigma'} \\ & + t\sum_{\mathbf{k}\sigma}[c^{\dagger}_{\mathbf{k}2\sigma}c_{\mathbf{k}1\sigma} + c^{\dagger}_{\mathbf{k}1\sigma}c_{\mathbf{k}2\sigma}] \\ & - U\sum_{\mathbf{k},\mathbf{k}',i} c^{\dagger}_{\mathbf{k}i\uparrow}c^{\dagger}_{-\mathbf{k}i\downarrow}c_{-\mathbf{k}'i\downarrow}c_{\mathbf{k}'i\uparrow}, \end{aligned} \tag{1}$$

where $c_{\mathbf{k}i\sigma}$ is the fermion annihilation operator with the momentum $\mathbf{k} = (k_x, k_y)$, layer index $i = 1, 2$, and spin $\sigma = \uparrow, \downarrow$. $\epsilon_{\mathbf{k}} = \mathbf{k}^2/(2m) - \mu$, Γ are the dispersion of free particles with mass m measured from the chemical potential μ and Zeeman field, respectively. t is the spin independent tunneling between two layers and U is the strength of attractive contact interaction. $\rho_{\mathbf{k}i}$ is the specified SOC for the ith layer with $\rho_{\mathbf{k}1} = \alpha k_y\sigma_x - \beta k_x\sigma_y$ and $\rho_{\mathbf{k}2} = -\alpha k_y\sigma_x - \beta k_x\sigma_y$, where α, β represent the strength of SOC and $\sigma_{x,y,z}$ are the Pauli matrices acting on the spin space. One feature of $\rho_{\mathbf{k}i}$ is π (0) phase difference for SOC along k_y (k_x) direction. When $\alpha = \beta$, $\rho_{\mathbf{k}1}$ corresponds to Rashba SOC, while $\rho_{\mathbf{k}2}$ corresponds to Dresselhaus SOC. Some forms of SOC in the bilayer systems have been suggested theoretically, including integration of $1d$ SOC in a different direction for different layer [35], Rashba SOC [36], and $1d$ SOC between the layer states [37]. Experimentally the equal weight of Rashba and Dresselhaus SOC [5–8,38] and $2d$ Rashba SOC [12,13,39] have been successfully realized. Considering highly controllability and tremendous progress in manipulating cold atom systems, SOC required in the model (1) is also in prospect.

The scattering between atoms can be treated in the mean field approximation and we assume that the two layers have the pairings $\Delta_i = U\sum_{\mathbf{k}}\langle c_{-\mathbf{k}i\downarrow}c_{\mathbf{k}i\uparrow}\rangle$, where $\langle\cdots\rangle$ means thermodynamic average. Under the Nambu basis $\Phi_{\mathbf{k}} = (\Psi_{\mathbf{k}}, \Psi^{\dagger}_{-\mathbf{k}})^T$ with $\Psi_{\mathbf{k}} = (c_{\mathbf{k}1\uparrow}, c_{\mathbf{k}1\downarrow}, c_{\mathbf{k}2\uparrow}, c_{\mathbf{k}2\downarrow})$, the Hamiltonian (1) can be arranged into $H = \frac{1}{2}\sum_{\mathbf{k}}\Phi^{\dagger}_{\mathbf{k}}H_{BdG}(\mathbf{k})\Phi_{\mathbf{k}}$ with

$$H_{BdG}(\mathbf{k}) = \begin{pmatrix} \mathcal{H}_0(\mathbf{k}) & \hat{\Delta} \\ \hat{\Delta}^{\dagger} & -\mathcal{H}^*_0(-\mathbf{k}) \end{pmatrix}, \tag{2}$$

where $\mathcal{H}_0(\mathbf{k}) = \epsilon_{\mathbf{k}} + \Gamma\sigma_z + ts_x + \alpha k_y s_z\sigma_x - \beta k_x\sigma_y$ and $\hat{\Delta} = -(i/2)[\Delta_1(s_0 + s_z) + \Delta_2(s_0 - s_z)]\sigma_y$. $s_{0,x,y,z}$ are Pauli matrices acting on the layer space. We will also introduce $\tau_{0,x,y,z}$ as Pauli matrices acting on the particle-hole space. The BdG Hamiltonian $H_{BdG}(\mathbf{k})$ has inherent particle-hole symmetry $\mathcal{P}H_{BdG}(\mathbf{k})\mathcal{P}^{-1} = -H_{BdG}(-\mathbf{k})$ with $\mathcal{P} = \tau_x K$ and inversion symmetry (IS) $\mathcal{I}H_{BdG}(\mathbf{k})\mathcal{I}^{-1} = H_{BdG}(-\mathbf{k})$ with $\mathcal{I} = \tau_z\sigma_z$, where K implements the complex conjugate operation. The combination of these two symmetries ensures that the eigenvalues $E_{\mathbf{k}\eta}$ ($\eta = 1, 2, \ldots, 8$) of $H_{BdG}(\mathbf{k})$ are in pairs. The thermodynamic potential of this model at zero temperature can be written as

$$\Omega = \frac{1}{2}\sum_{\mathbf{k}}\left(4\epsilon_{\mathbf{k}} - \sum_{\eta=1}^{4}E_{\mathbf{k}\eta}\right) + \frac{|\Delta_1|^2 + |\Delta_2|^2}{U}. \tag{3}$$

Here $E_{\mathbf{k}\eta}$ are four positive eigenvalues of $H_{BdG}(\mathbf{k})$. Notice that the ultraviolet divergence of the thermodynamic potential needs to be regularized [40] using

$$\frac{1}{U} = \sum_{\mathbf{k}}\frac{1}{\mathbf{k}^2/m + \epsilon_b}. \tag{4}$$

Thus the binding energy ϵ_b serves as the major parameter to control the many-body interaction strength. The minimization of the thermodynamic potential directly determines two order parameters

$$\partial\Omega/\partial\Delta_i = 0, \tag{5}$$

while the conservation of particle number determines the chemical potential

$$n = -\partial\Omega/\partial\mu, \tag{6}$$

where n is the particle density. In the following we numerically solve these equations self-consistently. We define the Fermi momentum $k_F = \sqrt{n\pi}$ and the Fermi energy $E_F = k_F^2/(2m)$, which are used to rescale the momentum and energy, respectively, during the numerical simulation. In this calculation, a lot of initial values are randomly chosen and the free energy

$$F = \Omega + \mu n \tag{7}$$

is calculated after the convergence. We have chosen the minimal point of free energy as the true ground state.

III. MEAN-FIELD PHASE DIAGRAM AND BULK TOPOLOGY

Before the self-consistent calculation, we notice that the attractive interaction U supports the Cooper pairings between spin-up and spin-down fermions near the Fermi surface. In the absence of SOC, a large Zeeman field Γ will break spin degeneracy and superfluid pairings, which is the topic often alluded to as the Chandrasekhar-Clogston limit in ordinary s-wave superconductor [41,42]. But once SOC is introduced into the system, every single-particle state is the superimposed state of two spin components. Under this circumstance, the Zeeman field Γ cannot suppress completely the superfluid pairings [43–45]. This observation shows that the ground state of the Hamiltonian (1) should be a superfluid state with $\Delta_i \neq 0$ $(i = 1, 2)$. This claim matches the numerically exact results below.

The order parameters Δ_i $(i = 1, 2)$ are complex numbers in principle. However, the numerical results show these two order parameters have the same magnitudes and phases, and thus can be treated as real numbers simultaneously. When $\Delta_1 = \Delta_2 = \Delta$, $H_{BdG}(\mathbf{k})$ obtains an emergent time-reversal symmetry (TRS) $\mathcal{T}H_{BdG}(\mathbf{k})\mathcal{T}^{-1} = H_{BdG}(-\mathbf{k})$ with $\mathcal{T} = s_x K$, and two MSs $\mathcal{M}_x H_{BdG}(k_x, k_y)\mathcal{M}_x^{-1} = H_{BdG}(-k_x, k_y)$, $\mathcal{M}_y H_{BdG}(k_x, k_y)\mathcal{M}_y^{-1} = H_{BdG}(k_x, -k_y)$ with $\mathcal{M}_x = \tau_z s_x \sigma_z$ and $\mathcal{M}_y = s_x$. Thus the BdG Hamiltonian (2) belongs to BDI class with chiral operator $\mathcal{C} = \mathcal{T}\mathcal{P}$ in ten Altland-Zirnbauer symmetry classes [14,15].

The construction of the system's phase diagram generally depends on the analytic expressions for eigenvalues $E_{\mathbf{k}\eta}$, whose gap closings qualitatively describe the phase boundaries. However, these eigenvalues cannot be calculated analytically in the most general condition. Fortunately, we are able to study the band structures of the model by studying the determinant of the BdG Hamiltonian. The chiral symmetry ensures that the eigenvalues will come with pairs; thus

$$\mathrm{Det}[H_{BdG}(\mathbf{k})] \geqslant 0. \tag{8}$$

In the above equation, $\mathrm{Det}[H_{BdG}(\mathbf{k})] = 0$ corresponds to the gap closings or gapless excitations. The determinant of the Hamiltonian can be calculated very easily with the help of the chiral operator $\mathcal{C}$. Under the basis diagonalizing the chiral operator, the Hamiltonian can be written into the off-diagonal form

$$H_{BdG}(\mathbf{k}) \sim \begin{pmatrix} 0 & Q(\mathbf{k}) \\ Q^{\dagger}(\mathbf{k}) & 0 \end{pmatrix}, \tag{9}$$

with $Q(\mathbf{k}) = \mathcal{H}_0(\mathbf{k})(s_x \otimes \sigma_0) - \hat{\Delta}$. Thus the gapless excitations correspond to

$$\mathrm{Det}[Q(\mathbf{k})] = R(\mathbf{k}) + 8i\beta t \Delta k_x \epsilon_{\mathbf{k}} = 0, \tag{10}$$

with the real function $R(\mathbf{k}) = (\epsilon_{\mathbf{k}}^2 - t^2 - k_x^2\beta^2 - k_y^2\alpha^2 - \Gamma^2 + \Delta^2)^2 - 4t^2(k_x^2\beta^2 + \Gamma^2) + 4(t^2 + k_x^2\beta^2 + k_y^2\alpha^2)\Delta^2$. Geometrically $R(\mathbf{k}) = 0$ defines a curve in the momentum space, similarly for $k_x\epsilon_{\mathbf{k}} = 0$. When these two curves cross, the system owns gapless excitations at some separated momenta; contrarily the system is gapped. We also differentiate the gapless phases from the number n_d of gapless points. From this criterion, the phase diagram of the model is constructed in Fig. 1.

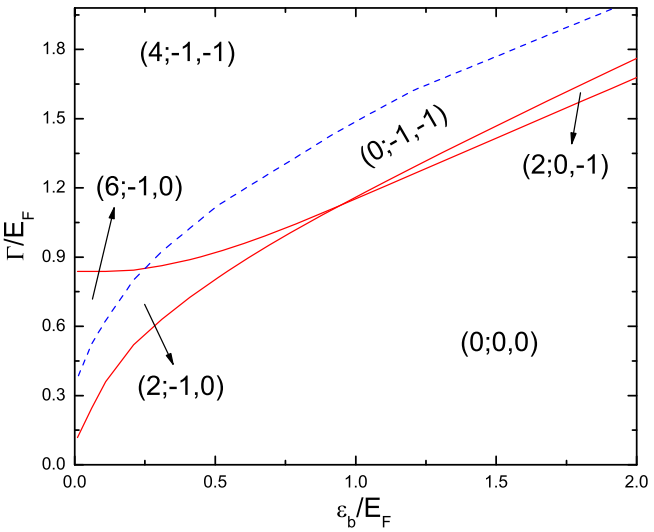

FIG. 1. Phase diagram of the model (2). The two solid phase boundaries mean that the energy gap closings and reopenings take place at $\mathbf{k} = 0$ and the dashed one means the gap closing and reopening at $k_x = 0$ and $k_y \neq 0$. Every phase in the phase diagram is labeled by the ordered number $(n_d; w_m^1, w_m^2)$, where n_d is the number of Dirac points and $w_m^{1,2}$ are the topological winding numbers in two mirror subspaces $\mathcal{M}_x^{1,2}$. The parameters are $t = 0.5E_F$ and $k_F\alpha = k_F\beta = 1.0E_F$.

Totally there are two gapped phases and three gapless phases with two, four, and six gapless nodal points, which are separated by three lines in the phase diagram. Two solid lines correspond to gap closings at $\mathbf{k} = 0$, leading to

$$\Gamma^2 = (\mu \pm t)^2 + \Delta^2. \tag{11}$$

When $\mu = 0$, these two lines cross, as demonstrated in Fig. 1; for the dashed phase boundary, the gap closing happens at $k_x = 0$, $k_y \neq 0$. Generally the topological phase boundaries always correlate with gap closings at zero momentum; thus our model supplies a counterintuitive example. When $t = 0$, two layers decouple and the phase boundaries (11) degenerate into the usual situation for the single layer [46,47].

In the gapless phases, the dispersions are linear near these nodal points (see Fig. 2); thus these gapless points are Dirac typed and protected by the topological winding numbers [48–51]

$$w = \frac{1}{2\pi}\mathrm{Im}\left[\oint_{\mathcal{L}} d\mathbf{k}\, \partial_{\mathbf{k}} \ln \mathrm{Det}[Q(\mathbf{k})]\right], \tag{12}$$

where the loop $\mathcal{L}$ encircles a Dirac point and Im means taking the imaginary part. The TRS requires $\mathrm{Det}[Q^*(\mathbf{k})] = \mathrm{Det}[Q(-\mathbf{k})]$; as a result the two Dirac points with opposite momenta have different winding numbers. The neutrality of topological charges in the entire space means even number of Dirac points.

Two gapped phases in the phase diagram are walled off from the gapless phases with two Dirac points. According to the Periodic Table of topological phases [14,15], a $2d$ gapped BDI class without other symmetries is topologically trivial. However, the existence of MSs can fundamentally change this conclusion [31–34]. To this end, we can diagonalize the mirror

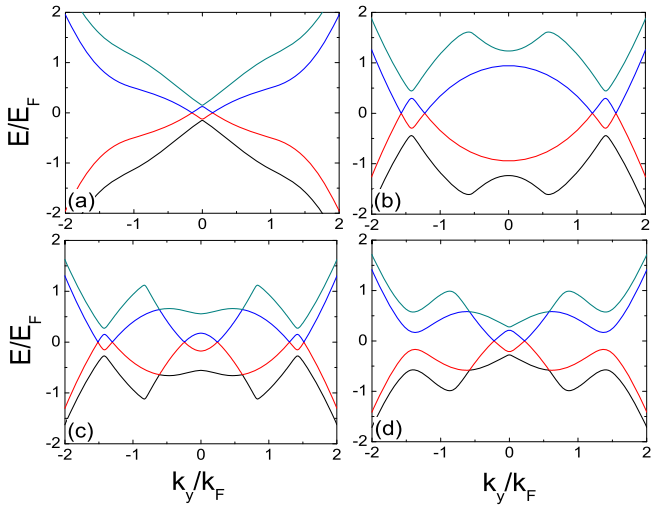

FIG. 2. Dispersions in gapless phases. Since all Dirac points locate on k_y axis, we plot $1d$ dispersions at $k_x = 0$. Panels (a)–(d) correspond to phases $(2; 0, -1)$, $(4; -1, -1)$, $(6; -1, 0)$, and $(2; -1, 0)$ in Fig. 1, respectively. In (a) $\epsilon_b = 1.91E_F$, $\Gamma = 1.68E_F$; in (b) $\epsilon_b = 0.81E_F$, $\Gamma = 1.6E_F$; in (c) $\epsilon_b = 0.06E_F$, $\Gamma = 0.7E_F$; in (d) $\epsilon_b = 0.21E_F$, $\Gamma = 0.65E_F$. The remaining parameters are $t = 0.5E_F$ and $k_F\alpha = k_F\beta = 1.0E_F$.

symmetry operator $\mathcal{M}_x$ ($\mathcal{M}_y$) via a unitary transformation; under the same transformation, $1d$ BdG Hamiltonian $H_y = H_{BdG}(k_x = 0, k_y)$ [$H_x = H_{BdG}(k_x, k_y = 0)$] can be arranged into block-diagonal form $H_{y,x} \sim \text{diag}(M^1_{y,x}, M^2_{y,x})$. In general $M^{1,2}_{x,y}$ can have totally different symmetries from the original Hamiltonian $H_{BdG}(\mathbf{k})$. For our model, only the mirror subspaces generated by $\mathcal{M}_y$ are important and

$$M^{1,2}_x = -(\epsilon_{k_x,k_y=0} \pm t)s_z + \Gamma s_z\sigma_z - \beta k_x s_z\sigma_y - \Delta s_y\sigma_y. \quad (13)$$

These two Hamiltonians have the same time-reversal operator $\mathcal{T}_m = K$ and particle-hole operator $\mathcal{P}_m = s_x \otimes \sigma_0 K$, and thus they belong to BDI class with chiral operator $\mathcal{C}_m = s_x \otimes \sigma_0$. On the other hand, $M^{1,2}_y$ belong to AI class, which are trivial in $1d$ and not listed.

As we have claimed that (10) is satisfied only at $k_x = 0$, thus (11) are also the gap closing conditions in mirror subspaces $M^{1,2}_x$, with $\pm$ mapped onto two subspaces. Furthermore, all gapless phases in the phase diagram are gapped in $M^{1,2}_x$. Here we notice that the gapless points in mirror subspaces must be the gapless points of $H_{BdG}(\mathbf{k})$, but it is not definitely correct contrarily. From the structure of the phase diagram, we can expect that there are luxuriant topologies in mirror subspaces. By means of $\mathcal{C}_m$ and following the procedure deriving Eq. (9), the mirror Hamiltonians can be transformed into

$$M^{1,2}_x \sim \begin{pmatrix} 0 & Q^{1,2}_x(k_x) \\ Q^{1,2\dagger}_x(k_x) & 0 \end{pmatrix}, \quad (14)$$

with $Q^{1,2}_x(k_x) = -(\epsilon_{k_x,k_y=0} \pm t)\sigma_0 + \Gamma\sigma_z - \beta k_x\sigma_y - i\Delta\sigma_y$. The topologies in mirror subspaces can be defined by the similar topological winding numbers [31–34] as in Eq. (12) by substituting Q into $Q^{1,2}_x$ and the integral over momentum loop into the whole Brillouin zone

$$w^{1,2}_m = \frac{1}{2\pi}\text{Im}\left[\int_{-\infty}^{\infty} dk_x \partial_{k_x} \ln \text{Det}[Q^{1,2}_x(k_x)]\right]. \quad (15)$$

Here we should note that the mirror winding numbers $w^{1,2}_m$ are independent. For this reason the mirror topological properties are labeled by two integer numbers (w^1_m, w^2_m).

The results for mirror winding numbers for all phases in the phase diagram are summarized as follows. The left (right) phase with two Dirac points has $(w^1_m, w^2_m) = (-1, 0)$ $[(0, -1)]$; the regime with four Dirac points has $(w^1_m, w^2_m) = (-1, -1)$; the gapless phase with six Dirac points has $(w^1_m, w^2_m) = (-1, 0)$; the higher (lower) fully gapped topological phase has $(w^1_m, w^2_m) = (-1, -1)$ [(0,0)]. Thus in addition to a trivial gapped phase, all phases in the phase diagram have nontrivial mirror topologies and can be distinguished by the ordered numbers $(n_d; w^1_m, w^2_m)$ from the number of Dirac points and topological winding numbers in two mirror subspaces. Here an interesting conclusion is that gapless nodal TSs can be topologically nontrivial in the mirror subspaces.

IV. BULK-BOUNDARY CORRESPONDENCE AND TS2

In order to consider the boundary states along an arbitrary direction, we first rotate the BdG Hamiltonian $H_{BdG}(\mathbf{k})$ in k_xk_y frame into $k_{x'}k_{y'}$ frame by an in-plane rotation with θ. Thus the momentum $\mathbf{k}$ is related to $\mathbf{k}'$ by the relations $k_x = k_{x'}\cos\theta - k_{y'}\sin\theta$ and $k_y = k_{y'}\cos\theta + k_{x'}\sin\theta$. We consider a strip with periodic boundary condition in y' direction and a finite width L_x along x' direction. In order to obtain the boundary states, we replace $k_{x'} \to -i\partial_{x'}$ and expand the wave function $\Phi(x') = \sqrt{\frac{2}{L_x}}\sum_{i=1}^{N_x} c_i \sin\frac{i\pi x'}{L_x}$ to convert the original Hamiltonian (2) into an $8N_x \times 8N_x$ boundary Hamiltonian [52], where c_i are eight-component spinors and N_x is basis cutoff. Diagonalizing this boundary Hamiltonian, boundary state spectra for all topological phases can be obtained, as shown in Fig. 3.

The dispersions of boundary states show different features. For the gapless phases, we can find dispersionless MFBs as long as $\theta \neq \pi/2$, which are used to connect the two Dirac points with opposite winding numbers. The MFB is a general feature in all nodal superconducting phases. The observed MFBs can be easily seized in a dimension reduction manner by calculating $k_{y'}$-dependent topological winding number [49–51]

$$w(k_{y'}) = \frac{1}{2\pi}\text{Im}\left[\int_{-\infty}^{\infty} dk_{x'} \partial_{k_{x'}} \ln \text{Det}[Q(\mathbf{k}')]\right], \quad (16)$$

as long as $k_{y'}$ does not cross the nodal points in momentum space. The MFBs in phases with two and six Dirac points cover $k_{y'} = 0$, while it is not true for a gapless phase with four Dirac points. This directly leads to their different boundary states at $\theta = 0$ since the nontrivial mirror topologies signify that there are linearly dispersive MZMs at $k_{y'} = k_y = 0$. The nontrivial mirror topologies also bring linearly dispersive MZMs for the gapped phase when $\theta = 0$. These MZMs will open a gap when θ deviates from mirror-invariant boundaries, as shown in Fig. 3(b) and Fig. 3(d). Finally, we emphasize that the mirror topologies are solely determined by the index

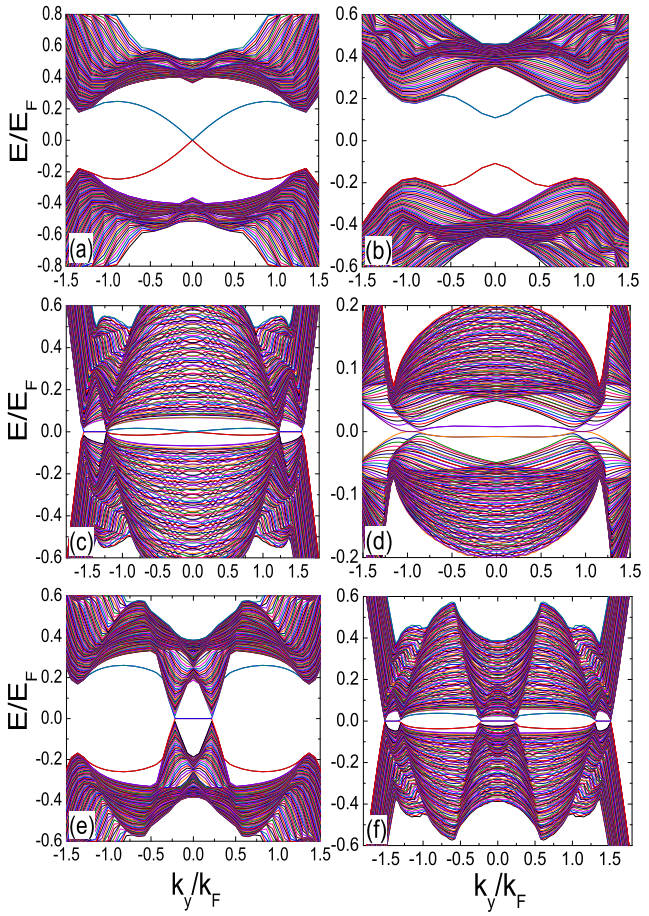

FIG. 3. Spectra of $1d$ boundary states. Panels (a) and (b), (c) and (d), (e), and (f) correspond to phases $(0;-1,-1)$, $(4;-1,-1)$, $(2;-1,0)$, and $(6;-1,0)$ in Fig. 1, respectively. In (a), (c), (e), and (f) $\theta=0$, while in (b) and (d) $\theta=\pi/4$. We don't show boundary state spectra in phases $(2;-1,0)$ and $(6;-1,0)$ for $\theta=\pi/4$, since MFBs in these phases have the similar forms with $\theta=0$. In (a) and (b) $\epsilon_b=0.81E_F$, $\Gamma=1.2E_F$; in (c) and (d) $\epsilon_b=0.81E_F$, $\Gamma=1.6E_F$; in (e) $\epsilon_b=0.21E_F$, $\Gamma=0.65E_F$; in (f) $\epsilon_b=0.06E_F$, $\Gamma=0.7E_F$. The remaining parameters are $t=0.5E_F$ and $k_F\alpha=k_F\beta=1.0E_F$.

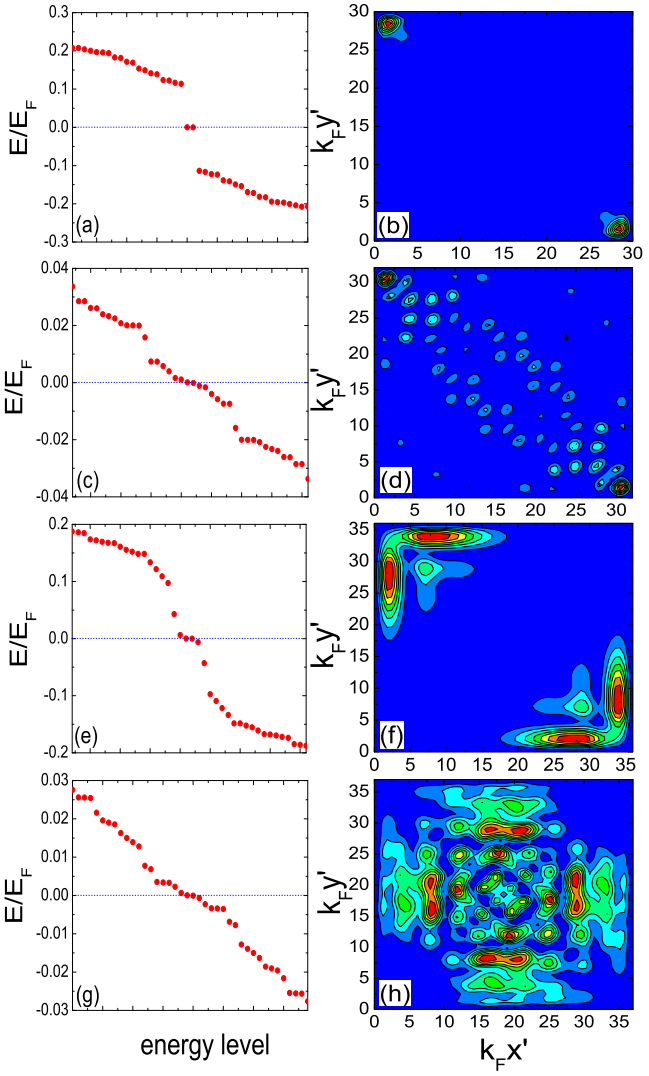

FIG. 4. Spectra of $0d$ boundary states and the wave functions of MZMs. (a) and (b), (c) and (d), (e) and (f), and (g) and (h) correspond to phases $(0;-1,-1)$, $(4;-1,-1)$, $(2;-1,0)$, and $(6;-1,0)$ in Fig. 1, respectively. We consider $\theta=\pi/4$ with the boundaries along x' and y' directions mapped onto each other under mirror symmetry. The parameters in the corresponding phases are the same as those in Fig. 3.

(w_m^1, w_m^2), while the observed MZMs at $k_{y'}=k_y=0$ generally originate from the combination of two mirror subspaces. Thus for phases only with a nonzero $w_m^{1,2}$, MZMs at $k_{y'}=k_y=0$ have definite mirror indices. However, in gapless phase with four Dirac points and topological gapped phase, this conclusion is not correct.

Below we discuss the MCSs in our model. At this time we impose open boundary conditions along x' and y' directions and expand the wave function $\Phi(x',y')=\sqrt{\frac{4}{L_xL_y}}\sum_{i=1}^{N_x}\sum_{j=1}^{N_y}c_{i,j}\sin\frac{i\pi x'}{L_x}\sin\frac{j\pi y'}{L_y}$, where L_y and N_y are the width and basis cutoff in y' direction, respectively. We consider $\theta=\pi/4$ with the boundaries along x' and y' directions mapped onto each other under mirror symmetry. For the topological gapped phase, the mirror topologies of the bulk guarantee that the boundary states in the specified configuration are gapped and the mirror-symmetry-breaking mass terms on these boundaries exhibit gaps of opposite signs [23,25]. As a result, the intersection of such boundaries corresponds to a domain wall and naturally leads to MCSs. The corresponding energy spectrum and wave function of MCSs in the topological gapped phase are shown in Figs. 4(a) and 4(b), consistent with the theory in [23,25]. In the gapless phase with four Dirac points, the gap of boundary states at $k_{y'}=0$ is also opened, similarly as the gapped topological phase. But the existence of MFBs on the boundaries causes the related energy spectrum [Fig. 4(c)] to show a series of low energy states besides MZMs. These low energy states directly lead to the leakage of MZMs into the interior of the system [Fig. 4(d)]. The energy spectra and corresponding wave functions for all other gapless phases are also plotted in Fig. 4 and show the consistent conclusions with the case in the gapless phase with four Dirac points. However, we note

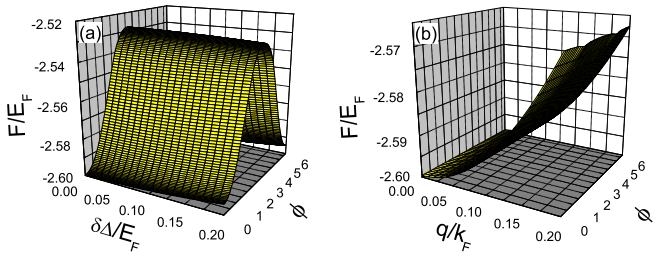

FIG. 5. Landscapes of free energy for phase $(0;-1,-1)$. Panels (a) and (b) correspond to *Ansätze* (i) and (ii) in the main text, respectively. The parameters are the same as those in Fig. 3. The other phases also have similar results.

that for the gapless phases with two Dirac points the number of low energy states is relatively small and the leakages of MZMs are not profound. Qualitatively the number of low energy states is consistent with the total width of MFBs in the momentum space. This naturally illustrates the small number of low energy states in gapless phases with two Dirac points.

V. DISCUSSION

The conclusions of MS protected gapped TS and TS2 not only depend on whether the order parameters Δ_i $(i=1,2)$ for two layers are equivalent, but also depend on spatially homogeneous property of superfluid states. If these two conditions are not satisfied, the emergent TRS and MS will be broken; as a result the topological protection of superfluid states will be destroyed. In order to exclude these possibilities, without loss of generality we consider two *Ansätze:* (i) $\Delta_1=\Delta$, $\Delta_2=(\Delta+\delta\Delta)e^{i\phi}$ with $\delta\Delta$, ϕ denoted respectively by magnitude and phase deviations from Δ_1 and (ii) $\Delta_1=\Delta_2=\Delta e^{iq(\cos\phi x+\sin\phi y)}$ with pairing momentum $\mathbf{q}=(q\cos\phi, q\sin\phi)$ to investigate the behavior of free energy F as the function of $\delta\Delta$, ϕ in *Ansatz* (i) and q, ϕ in *Ansatz* (ii) by self-consistently solving order parameter Δ and chemical potential μ. We find that the free energies increase for both cases. Figure 5 shows the landscapes of free energy for phase $(0;-1,-1)$. The other phases also have similar results. These numerical checks further address the validity of our results in the suggested system. As a matter of fact, in the present model the strong SOC is considered in the x and y direction, which could suppress the finite-momentum pairings along these directions [53,54].

In the theory of topological insulator, the presence of IS greatly simplifies the calculation of Z_2 invariant [55,56]. The BdG model (2) we consider also has IS, so the Hamiltonian commutes with inversion operator $\mathcal{I}$ and can be diagonalized simultaneously for time-reversal-invariant momentum $\mathbf{k}=0$. Note that for our model, except at the critical lines (11), the conduction bands and valence bands do not degenerate at $\mathbf{k}=0$; thus the sum of parity eigenvalues of valence bands is invariant for every phase. Due to phases $(0;-1,-1)$ and $(4;-1,-1)$ being separated by dashed line in Fig. 1, on which gap closing happens at $\mathbf{k}\neq 0$, these two phases have the same sum of parity eigenvalues for valence bands. This conclusion also applies to phases $(2;-1,0)$ and $(6;-1,0)$. In addition,

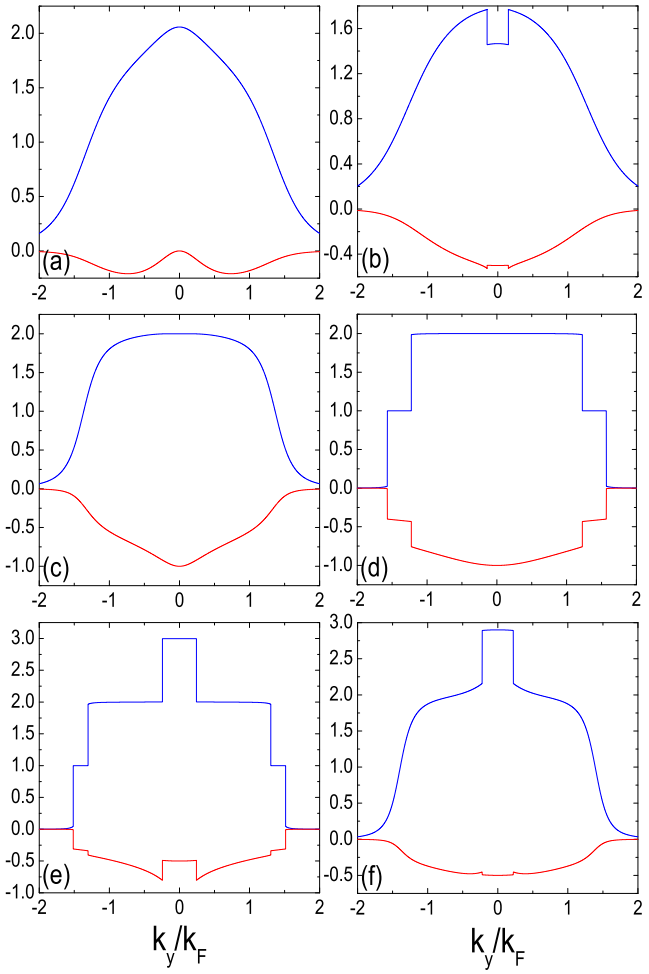

FIG. 6. Exotic behaviors of spin $S_z(k_y)$ [the red (lower) line] and particle's momentum distribution $n(k_y)$ [the blue (upper) line] along k_y for all phases. Panels (a)–(f) correspond to phases $(0;0,0)$, $(2;0,-1)$, $(0;-1,-1)$, $(4;-1,-1)$, $(6;-1,0)$, and $(2;-1,0)$, respectively. In (a) $\epsilon_b=0.81E_F$ and $\Gamma=0.85E_F$; in (c) $\epsilon_b=0.81E_F$ and $\Gamma=1.2E_F$. The parameter of gapless phases are the same as those in Fig. 2.

phases $(2;-1,0)$ and $(2;0,-1)$ also have the same sum of parity eigenvalues since they can be obtained from the phase $(0;0,0)$ by gap closings at $\mathbf{k}=0$. Accidentally, the spin operator $\hat{S}_z(\mathbf{k})=\mathcal{I}/4$, so that its expectation value $S_z(\mathbf{k})$ is also conserved at $\mathbf{k}=0$ and equal to the sum of parity eigenvalues for valence bands divided by 4. We find that $S_z(0)=0$, $-\frac{1}{2}$, -1 for phases $(0;0,0)$, $(6;-1,0)$, $(0;-1,-1)$, respectively. For general momentum, the analyses above do not validate and $S_z(\mathbf{k})$ is not quantized. But in the gapless phases, the conduction bands contact with valence bands at Dirac points, which should affect the spin behaviors near the Dirac points. In order to testify to this claim, in Fig. 6 we plot $S_z(k_x=0,k_y)=S_z(k_y)$ along k_y axis for all phases and find that $S_z(k_y)$ shows discontinuous changes near all Dirac points. In Fig. 6 we also plot particle's momentum distribution $n(k_x=0,k_y)=n(k_y)$, which also has similar behaviors with $S_z(k_y)$. These different exotic behaviors on $S_z(k_y)$ and $n(k_y)$ will provide unique fingerprints to experimentally identify all phases by

the most powerful time-of-flight imaging technique in the ultracold atom environment.

The different band structures of the corresponding phases shown in Fig. 2 can also be detected by momentum-resolved radio-frequency spectroscopy [57–59], which has been widely used to study BCS-BEC crossover [60–62] and polarons [63,64] in spin-imbalanced Fermi gases. Moreover, this technique provides an analog to angle-resolved photoemission spectroscopy (ARPES) in the condensed-matter physics [62].

VI. CONCLUSION

In conclusion, we suggest a theoretic model to realize MS-protected gapped TS and TS2. On one hand, this gapped phase is protected by nonlocal unitary symmetry, but not local antiunitary symmetry in ten Altland-Zirnbauer symmetry classes. On the other hand, this phase also realizes TS2 with conventional s-wave pairing, signifying that, in addition to pairing symmetry, the single-particle band structures provide another knob to engineer TS2. By the self-consistent calculation we also find some gapless TSs. All phases can be distinguished from the number of Dirac points and topological winding numbers in two mirror subspaces. An interesting conclusion is that gapless nodal TSs can be topologically nontrivial in the mirror subspaces. These TSs show linearly dispersive MZMs, MFBs, and even their coexistence, depending on corresponding bulk phases and $(d-1)$-dimensional boundary configurations. On the other hand for $(d-2)$-dimensional boundaries, these phases also accommodate MZMs. For the gapped TS, these MZMs are spatially localized around the corners to realize MCSs, while, for gapless TSs, the wave functions of MZMs more or less leak into the interior of the system in virtue of MFBs on the $(d-1)$-dimensional boundaries. Our model can be mapped to a bilayer model in the cold fermionic gases with π (0) phase difference for SOC along k_y (k_x) direction between two layers. Considering the tremendous progress in manipulating cold atom systems, our work provides a possible route to realize MS-protected TSs and TS2 in cold fermionic systems in the future.

ACKNOWLEDGMENTS

B.H. acknowledges stimulating discussions with Ming Gong. This work is supported by National Natural Science Foundation of China (Grants No. 11547047 and No. 11504038), the Natural Science Foundation of Jiangsu Province (Grant No. BK20150423), the Industry-University-Research cooperation project of Jiangsu province (No. BY2018273), and Chongqing Fundamental, Frontier Research Program (No. cstc2015jcyjA00013).

[1] E. Majorana, Nuovo Cimento **14**, 171 (1937).
[2] C. Nayak, S. H. Simon, A. Stern, M. Freedman, and S. Das Sarma, Rev. Mod. Phys. **80**, 1083 (2008).
[3] X.-L. Qi and S.-C. Zhang, Rev. Mod. Phys. **83**, 1057 (2011).
[4] M. Z. Hasan and C. L. Kane, Rev. Mod. Phys. **82**, 3045 (2010).
[5] Y.-J. Lin, K. Jiménez-García, and I. B. Spielman, Nature (London) **471**, 83 (2011).
[6] J. Y. Zhang, S. C. Ji, Z. Chen, L. Zhang, Z.-D. Du, B. Yan, G.-S. Pan, B. Zhao, Y.-J. Deng, H. Zhai, S. Chen, and J.-W. Pan, Phys. Rev. Lett. **109**, 115301 (2012).
[7] L. W. Cheuk, A. T. Sommer, Z. Hadzibabic, T. Yefsah, W. S. Bakr, and M. W. Zwierlein, Phys. Rev. Lett. **109**, 095302 (2012).
[8] P. Wang, Z.-Q. Yu, Z. Fu, J. Miao, L. Huang, S. Chai, H. Zhai, and J. Zhang, Phys. Rev. Lett. **109**, 095301 (2012).
[9] R. A. Williams, M. C. Beeler, L. J. LeBlanc, K. Jiménez-García, and I. B. Spielman, Phys. Rev. Lett. **111**, 095301 (2013).
[10] C. Hamner, Y. Zhang, M. A. Khamehchi, M. J. Davis, and P. Engels, Phys. Rev. Lett. **114**, 070401 (2015).
[11] K. Jiménez-García, L. J. LeBlanc, R. A. Williams, M. C. Beeler, C. Qu, M. Gong, C. Zhang, and I. B. Spielman, Phys. Rev. Lett. **114**, 125301 (2015).
[12] L. Huang, Z. Meng, P. Wang, P. Peng, S.-L. Zhang, L. Chen, D. Li, Q. Zhou, and J. Zhang, Nat. Phys. **12**, 540 (2016).
[13] Z. Wu, L. Zhang, W. Sun, X.-T. Xu, B.-Z. Wang, S.-C. Ji, Y. Deng, S. Chen, X.-J. Liu, and J.-W. Pan, Science **354**, 83 (2016).
[14] A. P. Schnyder, S. Ryu, A. Furusaki, and A. W. W. Ludwig, Phys. Rev. B **78**, 195125 (2008); in *Advances in Theoretical Physics: Landau Memorial Conference*, edited by V. Lebedev and M. Feigel'man, AIP Conf. Proc. No. 1134 (AIP, Melville, NY, 2009), p. 10.
[15] A. Y. Kitaev, in *Advances in Theoretical Physis: Landau Memorial Conference*, edited by V. Lebedev and M. Feigel'ma, AIP Conf. Proc. No. 1134 (Ref. [14]), p. 22.
[16] C. Zhang, S. Tewari, R. M. Lutchyn, and S. Das Sarma, Phys. Rev. Lett. **101**, 160401 (2008).
[17] M. Sato, Y. Takahashi, and S. Fujimoto, Phys. Rev. Lett. **103**, 020401 (2009).
[18] C. Qu, Z. Zheng, M. Gong, Y. Xu, L. Mao, X. Zou, G. Guo, and C. Zhang, Nat. Commun. **4**, 2710 (2013).
[19] W. Zhang and W. Yi, Nat. Commun. **4**, 2711 (2013).
[20] Y.-C. Zhang, Z. Xu, and S. Zhang, Phys. Rev. A **95**, 043640 (2017).
[21] J. M. Midtgaard, Z. Wu, and G. M. Bruun, Phys. Rev. A **96**, 033605 (2017).
[22] J. C. Y. Teo and T. L. Hughes, Phys. Rev. Lett. **111**, 047006 (2013).
[23] J. Langbehn, Y. Peng, L. Trifunovic, F. von Oppen, and P. W. Brouwer, Phys. Rev. Lett. **119**, 246401 (2017).
[24] E. Khalaf, Phys. Rev. B **97**, 205136 (2018).
[25] M. Geier, L. Trifunovic, M. Hoskam, and P. W. Brouwer, Phys. Rev. B **97**, 205135 (2018).
[26] X. Zhu, Phys. Rev. B **97**, 205134 (2018).
[27] H. Shapourian, Y. Wang, and S. Ryu, Phys. Rev. B **97**, 094508 (2018).
[28] Q. Wang, C.-C. Liu, Y.-M. Lu, and F. Zhang, Phys. Rev. Lett. **121**, 186801 (2018).
[29] Y. Wang, M. Lin, and T. L. Hughes, Phys. Rev. B **98**, 165144 (2018).

[30] Z. Yan, F. Song, and Z. Wang, Phys. Rev. Lett. **121**, 096803 (2018).
[31] C.-K. Chiu, H. Yao, and S. Ryu, Phys. Rev. B **88**, 075142 (2013).
[32] H. Yao and S. Ryu, Phys. Rev. B **88**, 064507 (2013).
[33] Y. Ueno, A. Yamakage, Y. Tanaka, and M. Sato, Phys. Rev. Lett. **111**, 087002 (2013).
[34] K. Shiozaki and M. Sato, Phys. Rev. B **90**, 165114 (2014).
[35] Q. Sun, L. Wen, W.-M. Liu, G. Juzeliūnas, and A.-C. Ji, Phys. Rev. A **91**, 033619 (2015).
[36] S.-W. Su, S.-C. Gou, Q. Sun, L. Wen, W.-M. Liu, A.-C. Ji, J. Ruseckas, and G. Juzeliūnas, Phys. Rev. A **93**, 053630 (2016).
[37] Q. Sun, L.-L. Wang, X.-J. Liu, G. Juzeliūnas, and A.-C. Ji, Phys. Rev. A **99**, 043601 (2019).
[38] J. Li, W. Huang, B. Shteynas, S. Burchesky, F. Ç. Top, E. Su, J. Lee, A. O. Jamison, and W. Ketterle, Phys. Rev. Lett. **117**, 185301 (2016).
[39] W. Sun, B.-Z. Wang, X.-T. Xu, C.-R. Yi, L. Zhang, Z. Wu, Y. Deng, X.-J. Liu, S. Chen, and J.-W. Pan, Phys. Rev. Lett. **121**, 150401 (2018).
[40] M. Randeria, J.-M. Duan, and L.-Y. Shieh, Phys. Rev. Lett. **62**, 981 (1989).
[41] B. S. Chandrasekhar, Appl. Phys. Lett. **1**, 7 (1962).
[42] A. M. Clogston, Phys. Rev. Lett. **9**, 266 (1962).
[43] S. Tewari, T. D. Stanescu, J. D. Sau, and S. Das Sarma, New J. Phys. **13**, 065004 (2011).
[44] J. Zhou, W. Zhang, and W. Yi, Phys. Rev. A **84**, 063603 (2011).
[45] J.-N. Zhang, Y.-H. Chan, and L.-M. Duan, arXiv:1110.2241.
[46] M. Gong, S. Tewari, and C. Zhang, Phys. Rev. Lett. **107**, 195303 (2011).
[47] M. Gong, G. Chen, S. Jia, and C. Zhang, Phys. Rev. Lett. **109**, 105302 (2012).
[48] Y. X. Zhao and Z. D. Wang, Phys. Rev. Lett. **110**, 240404 (2013).
[49] B. Béri, Phys. Rev. B **81**, 134515 (2010).
[50] M. Sato, Y. Tanaka, K. Yada, and T. Yokoyama, Phys. Rev. B **83**, 224511 (2011).
[51] B. Huang, X. Yang, N. Xu, and M. Gong, Phys. Rev. B **97**, 045142 (2018).
[52] B. Huang, C. F. Chan, and M. Gong, Phys. Rev. B **91**, 134512 (2015).
[53] T. Zhou, Y. Gao, and Z. D. Wang, Phys. Rev. B **93**, 094517 (2016).
[54] T. Zhou, Y. Gao, and Z. D. Wang, Sci. Rep. **4**, 5218 (2014).
[55] L. Fu and C. L. Kane, Phys. Rev. B **76**, 045302 (2007).
[56] Y. Ando, J. Phys. Soc. Jpn. **82**, 102001 (2013).
[57] Z. Fu, L. Huang, Z. Meng, P. Wang, X.-J. Liu, H. Pu, H. Hu, and J. Zhang, Phys. Rev. A **87**, 053619 (2013).
[58] J. Zhang, H. Hu, X.-J. Liu, and H. Pu, Fermi gases with synthetic spin-orbit coupling, in *Annual Review of Cold Atoms and Molecules*, Vol. 2 (Stallion, Singapore, 2014), p. 81.
[59] S.-G. Peng, X.-J. Liu, H. Hu, and K. Jiang, Phys. Rev. A **86**, 063610 (2012).
[60] C. Chin, M. Bartenstein, A. Altmeyer, S. Riedl, S. Jochim, J. Hecker Denschlag, and R. Grimm, Science **305**, 1128 (2004).
[61] C. H. Schunck, Y. Shin, A. Schirotzek, and W. Ketterle, Nature (London) **454**, 739 (2008).
[62] J. T. Stewart, J. P. Gaebler, and D. S. Jin, Nature (London) **454**, 744 (2008).
[63] C. Kohstall, M. Zaccanti, M. Jag, A. Trenkwalder, P. Massignan, G. M. Bruun, F. Schreck, and R. Grimm, Nature (London) **485**, 615 (2012).
[64] M. Koschorreck, D. Pertot, E. Vogt, B. Fröhlich, M. Feld, and M. Köhl, Nature (London) **485**, 619 (2012).